

# Multi-objective solution and decision-making framework for coordinating the short-term hydropeaking-navigation-production conflict of cascade hydropower reservoirs

Xiangyu Ma<sup>a</sup>, Shengli Liao<sup>a,\*</sup>, Benxi Liu<sup>a</sup>, Hongye Zhao<sup>a</sup>, Chuntian Cheng<sup>a</sup>, Huaying Su<sup>b</sup>

<sup>a</sup> Institute of Hydropower and Hydroinformatics, Dalian University of Technology, Dalian, 116024, China

<sup>b</sup> Electric Power Dispatching and Control Center of Guizhou Power Grid Co., Ltd., Guiyang, 550002, China



## ARTICLE INFO

Handling Editor: Mingzhou Jin

### Keywords:

Multi-objective optimal scheduling  
Peak shaving  
Cascade hydropower reservoirs  
Normalized normal constraint  
Mixed integer linear programming  
CW-TOPSIS

## ABSTRACT

The transformation of energy structure motivates hydropower to participate in peak shaving operations for grid stability, which conflicts with the multiple uses of cascade hydropower reservoirs. To coordinate the principal contradictory tasks of peak shaving, ship navigation, and power generation in day-ahead scheduling, a mixed integer linear programming model for the short-term multi-objective optimal scheduling is constructed. Specifically, a novel power release-based indicator is adopted to describe the navigation objective, while the minimization of the peak-valley difference of the residual load and the total water released are taken as the other two objective functions. Constraint aggregation and rectangular meshing methods are employed to handle the challenging nonlinear and nonconvex constraints. Subsequently, the Normalized Normal Constraint method, integrated with the mathematical optimization solver Gurobi, generates a set of well-distributed Pareto solutions, each representing a scheduling scheme. Finally, the Combined Weighting - Technique for Order Preference by Similarity to Ideal Solution is utilized as a decision-maker to trade off and determine a compromise solution for final implementation. Case studies on the cascade hydropower reservoirs of the Wujiang River in China demonstrate that the proposed model can adequately characterize the demands of various stakeholders, and the suggested framework can obtain an even and extensive Pareto front, mediate conflicts, and make reasonable decisions. Compared to the original peak-shaving scheme, the finalized compromise scheme reduces the peak-shaving effect by just 27.82% but offers simultaneous boosts of 96.54% in navigation benefits and 10.88% in power generation benefits. Consequently, the presented framework can be a promising alternative for conflict resolution of cascade hydropower reservoirs.

## 1. Introduction

Hydropower is an essential clean and renewable energy that ensures global decarbonization targets remain within reach (IHA, 2022). Due to their storage and adjustability, hydropower reservoirs offer multiple functions in addition to providing reliable electricity, such as flood control, ship navigation, environmental flows, and water supply, which can create conflicts in operation (Branche, E., 2017).

With the continuous growth of peak load and expected increasing share of variable renewables such as wind and solar, the pressure of power balancing is exacerbated, necessitating additional flexibility (Ding et al., 2015; Uddin et al., 2018). To support grid stability, it is promising for hydropower, a large-scale and well-dispatchable

renewable energy, to participate in peak shaving, i.e., hydropower peak shaving operation (HPSO) or hydropeaking (Kling, 2017; Zhou et al., 2020). HPSO is an operation mode in which cascade hydropower reservoirs (CHR) adjust the power output processes to track varying loads through their storage capacity and fast response characteristics (Sahin et al., 2017; Liao et al., 2021). However, this mode may not be optimal for other tasks of multi-purpose reservoirs or even have negative impacts, posing new challenges for hydropower operations. For power producers, HPSO may lead to lower generation efficiency, higher generation costs, or even avoidable water spillage (Shen et al., 2020; Zhang et al., 2020a). Additionally, HPSO can cause frequent fluctuations and rapid variations in downstream river flows and water levels, significantly affecting shipping conditions and ecosystem stability (Poff and Schmidt, 2016; Shang et al., 2017).

\* Corresponding author.

E-mail address: [shengliliao@dlut.edu.cn](mailto:shengliliao@dlut.edu.cn) (S. Liao).

<b>Nomenclature</b>	
<b>A. Acronyms</b>	
ANPRVI	Average normalized power release variation index
CCC	Centralized control center
CHR	Cascade hydropower reservoirs
CS	Compromise scheme
CW-TOPSIS	Combined weighting - Technique for Order Preference by Similarity to Ideal Solution
EHPF	Equivalent hydropower production function
FA	Firefly algorithm
HPSO	Hydropower peak shaving operation
HRND	Hydropower reservoir with navigation demand
INNC	Improved normalized normal constraint
MILP	Mixed integer linear programming
MOOP	Multi-objective optimization problem
MOOS	Multi-objective optimal scheduling
NNC	Normalized normal constraint
NPRVI	Normalized power release variation index
NSDE	Non-dominated sorting differential evolution
NSGA-II	Non-dominated sorting genetic algorithm II
OS	Original scheme
R-IMOMFO	R-domination-based improved multi-objective moth-flame optimization algorithm
SOOP	Single-objective optimization problem
SOS2	Special ordered sets of type two
SPEA2	Strength pareto evolutionary algorithm 2
STMOOS	Short-term multi-objective optimal scheduling
WGP	Weighted goal programming
WS	Weighted sum
<b>B. Indices</b>	
$n$	Index of hydropower reservoirs (or corresponding plants)
$t$	Index of time periods
<b>C. Sets</b>	
$N$	Set of indices of hydropower reservoirs (or corresponding plants)
$SN^D$	Set of indices of HRNDs, $SN^D \subseteq N$
$T$	Set of indices of time periods
<b>D. Variables</b>	
$D_t$	Original load demand of the power grid at period $t$ [MW]
$D_t^{res}$	Residual load demand of the power grid at period $t$ [MW]
$H_{n,t}$	Net head of hydropower plant $n$ at period $t$ [m]
$H_{n,t}^{loss}$	Head loss of hydropower plant $n$ at period $t$ [m]
$P_{n,t}$	Power output of hydropower plant $n$ at period $t$ [MW]
$Q_{n,t}^{in}$	Natural inflow of hydropower reservoir $n$ at period $t$ [ $m^3/s$ ]
$Q_{n,t}^{nor}$	Normalized power release of hydropower plant $n$ at period $t$
$Q_n^{nor}$	Average value of normalized power release of hydropower plant $n$ over the operation periods
$Q_{n,t}^{out}$	Water discharge of hydropower reservoir $n$ at period $t$ [ $m^3/s$ ]
<b>s]</b>	
$Q_{n,t}^{power}$	Power release of hydropower plant $n$ at period $t$ [ $m^3/s$ ]
$Q_{n,t}^{spill}$	Water spillage of hydropower reservoir $n$ at period $t$ [ $m^3/s$ ]
$V_{n,t}$	Water storage of hydropower reservoir $n$ at period $t$ [ $m^3$ ]
$Z_{n,t}$	Forebay water level of hydropower reservoir $n$ at period $t$ [m]
$Z_{n,t}^{tail}$	Tailwater level of hydropower reservoir $n$ at period $t$ [m]
$\Delta Z_n^d$	Daily variation of the tailwater level of plant $n$ [m]
$\Delta Z_{n,t}^h$	Hourly variation of the tailwater level of plant $n$ at period $t$ [m]
$\psi_t$	NPRVI of HRNDs at period $t$
$\bar{\psi}$	ANPRVI of HRNDs over the operation periods
<b>E. Constants</b>	
$E$	Total electricity demand for cascade hydropower plants over the scheduling periods [MW·h]
$N^D$	Number of HRNDs
$\bar{P}_n$	Upper bound of power output of hydropower plant $n$ [MW]
$\underline{P}_n$	Lower bound of power output of hydropower plant $n$ [MW]
$Q_n^{eco}$	Minimum ecological flow of hydropower reservoir $n$ [ $m^3/s$ ]
$Q_n^{navi}$	Minimum navigation flow of hydropower reservoir $n$ [ $m^3/s$ ]
$\bar{Q}_n^{out}$	Maximum water discharge of hydropower reservoir $n$ [ $m^3/s$ ]
$\underline{Q}_n^{out}$	Minimum water discharge of hydropower reservoir $n$ [ $m^3/s$ ]
$\bar{Q}_n^{power}$	Maximum power release of hydropower plant $n$ [ $m^3/s$ ]
$\underline{Q}_n^{power}$	Minimum power release of hydropower plant $n$ [ $m^3/s$ ]
$\bar{V}_n$	Upper bound of water storage in hydropower reservoir $n$ [ $m^3$ ]
$\underline{V}_n$	Lower bound of water storage in hydropower reservoir $n$ [ $m^3$ ]
$V_n^{init}$	Initial water storage in hydropower reservoir $n$ [ $m^3$ ]
$\Delta P_n$	Maximum power ramping capacity of hydropower plant $n$ [MW]
$\Delta t$	Duration of the time period [h], 0.25h
<b>F. Functions</b>	
$f_n^{loss}(\cdot)$	Function that specifies head loss and power release of hydropower plant $n$
$f_n^{phq}(\cdot)$	Two-dimensional power production function of hydropower plant $n$ with respect to the net head and power release of hydropower plant $n$
$f_n^{tail}(\cdot)$	Function that specifies tailwater level and water release of hydropower reservoir $n$
$f_n^{zv}(\cdot)$	Function that specifies forebay water level and storage of hydropower reservoir $n$
$\Gamma_n(\cdot)$	Equivalent hydropower production function (EHPF) of hydropower plant $n$

Anindito et al. (2019) investigated the prospective of using batteries and re-regulation reservoirs on hydropeaking mitigation. However, their short-term feasibility is constrained by cost, construction period, and technical limitations. Scholars have also proposed using operational constraints encompassing minimum flows and maximum ramps to alleviate negative hydropeaking impacts (Bruder et al., 2016). However, there is a lack of a clear criterion for determining hydropeaking flow thresholds that can balance peak-shaving flexibility with potential downstream benefits (Moreira et al., 2019).

Indeed, hydropower is at the heart of the water-energy nexus due to its unique role and multiple benefits in the water resource and energy systems (Branche, E., 2017). Effectively coordinating multiple stakeholders' interests and developing rational operation schemes is crucial, which is a typical multi-objective optimization problem (MOOP), known as the multi-objective optimal scheduling (MOOS) of CHR (Yang et al., 2020).

Due to existing conflicts, optimizing all objectives simultaneously in MOOP is difficult. Instead of a single optimal solution, MOOP generates

a set of optimal solutions known as Pareto solutions, collectively called the Pareto front. To sufficiently reveal trade-offs between objectives, numerous Pareto-based algorithms have emerged, which can be categorized into two types: vectorization and scalarization methods (Feng et al., 2017). The first type, such as non-dominated sorting genetic algorithm II (NSGA-II) (Zhang et al., 2019) and multi-objective particle swarm optimization (Yang et al., 2020), are primarily intelligent optimization algorithms that can directly handle a MOOP through different searching mechanisms. However, their application to large-scale problems is challenging due to the ballooning search space dimensions. As for scalarization methods, which transform MOOP into a series of single-objective optimization problems (SOOPs), the typical ones include weighted sum (WS),  $\epsilon$ -constraint (Shen et al., 2020), and normalized normal constraint (NNC) (Liao et al., 2022). By combining conventional optimization methods, they solve the transformed sub-SOOPs to obtain Pareto solutions, which makes them easy to implement. However, there are still drawbacks, such as the fact that WS is unable to obtain Pareto solutions with even distribution, and the results of selecting different main objective functions are significantly disparate in  $\epsilon$ -constraint method. In comparison, NNC can obtain a well-distributed Pareto front to efficiently describe the trade-off between objectives and has been widely used in various fields (Pereira et al., 2017). Additionally, Ghiasi et al. (2010) demonstrated that NNC outperforms classical NSGA-II in converging to the true Pareto front, making it more applicable to problems requiring an extensive Pareto front and with no high demands for the solution's quantity.

Extracting the best compromise solution from the Pareto front is a crucial step after solving MOOP. Scholars have proposed many decision-making approaches, such as fuzzy-based methods (Zhou et al., 2020) and problem-specific approaches like subjective trade-off rate (Wang et al., 2020). Either relying on subjective preferences or addressing particular problems, these approaches still have limitations. By contrast, multi-attribute decision-making (MADM) methods such as TOPSIS (Yu et al., 2021), VIKOR (Simab et al., 2018), COPRAS, and MULTIMOORA (Alkan and Albayrak, 2020) are practical and generalizable. With appropriate improvements, MADM can consider both subjective preferences and objective information and adapt to various problems (Chen, 2021).

Specific to the modeling, solution and decision-making for MOOS of CHR, scholars have attempted many studies thus far. The detailed analysis is as follows:

Zhang et al. (2020b) proposed the R-domination-based improved multi-objective moth-flame optimization algorithm (R-IMOMFO) to solve the MOOS model containing hydropower generation, ecology, and navigation objectives. The contradictory relationships were verified by analyzing the obtained Pareto solutions. Jia et al. (2019) established a STMOOS model taking into account navigation and power generation. The Pareto front generated by the strength pareto evolutionary algorithm (SPEA2) indicated an apparent inverse relationship between power generation and downstream navigation. Moura De Figueiredo et al. (2023) developed an optimization system based on nonlinear programming and weighted goal programming (WGP) to minimize conflicts arising from multiple water uses in hydropower reservoirs. Application on Brazil validates its efficiency in trade-offs analysis between power generation and navigation. Concentrating on the multiple uses of reservoirs, these studies explored the contradiction between

hydropower generation, navigation, and ecology. However, no attention was given to the HPSO task, and no final decision was made on the Pareto solutions.

Li et al. (2022) developed a conflict resolution model for reservoir operation considering hydropower generation and navigation. NSGA-II and two decision-maker preference-based methods, Conflict Averse and Hero, were used to solve and make decisions. Wang et al. (2022a) constructed a NSGA-II-based MOOS model involving power generation, hydropower output stability, and ecological demands. Then a Pareto front shrinking approach was proposed to reduce the selection range of Pareto solutions. These works further explored the decision-making methods for MOOS of CHR but still did not consider the peak shaving demand.

Zhou et al. (2020) presented a mixed-integer nonlinear programming model aiming to regulate peak loads and enhance power efficiency, with a fuzzy-based method employed to select the compromise solution from the Pareto front yielded by the improved normalized constraint (INNC) method. Shen et al. (2020) developed a MOOS model for a hydropower system to disclose conflicts between energy production and peak shaving, with an  $\epsilon$ -constraint method employed and a solution methodology presented for solving and determining the final scheme. From the perspective of hydropower and power system operation, these studies analyzed the peak-shaving operation of hydropower reservoirs or its contradiction with energy production but have neglected conflicts with providing navigation and ecological requirements.

Zhang et al. (2020a) proposed a STMOOS model to coordinate conflicts between new energy consumption, peak shaving demand, and discarded water of CHR. After decomposing the tri-objective model into two sub-models, the optimum solution was determined using firefly algorithm (FA) and fuzzy optimization method. To further improve the performance of hydro-wind-solar complementary systems, Guo et al. (2022) proposed a risk-averse model considering comprehensive risk rate, cascade hydropower production, and peak shaving performance. Then the non-dominated sorting differential evolution algorithm (NSDE) was employed to solve the model. These studies further studied the conflicts between the power generation of CHR and power system operation, such as peak shaving and energy complementary, yet again ignored other various tasks of CHR.

Gonzalez et al. (2023) developed a Borg MOEA-based multisector simulation model to optimize intermittent renewables integration while minimizing negative impacts caused by hydropeaking on river ecosystems and agricultural irrigation. Three problem-specific intervention strategies were proposed for decision-making. This study provides a useful tool for designing future renewable energy systems in Ghana. However, the hydropower operation was considered relatively simple without considering complex constraints such as water head effects, not yet suitable for current short-term fine scheduling.

The mentioned studies have extensively explored the modeling, solution, and decision-making methods for MOOS of CHR from the perspectives of water resource utilization and power system operation. A concise summary is provided in Table 1. However, few studies have considered the peak shaving for power grid and multiple uses of reservoirs simultaneously, particularly the notable conflicts between peak shaving, navigation, and power generation in day-ahead scheduling for CHR.

**Table 1**

A summary of related literature.

Reference	Objective Functions				Pareto-based solution methods	Decision-making methods
	Water resource allocation			Power system operation		
	Power Generation	Navigation	Ecology	Peak shaving	Energy Complementary	
Zhang et al. (2020b)	*	*	*		R-IMOMFO	
Jia et al. (2019)	*	*			SPEA2	
Moura De Figueiredo et al. (2023)	*	*	*			WGP
Li et al. (2022)	*	*			NSGA-II	
Wang et al. (2022a)	*		*		NSGA-II	
Zhou et al. (2020)	*			*		INNC $\epsilon$ -constraint
Shen et al. (2020)	*			*		Fuzzy-based membership Decision preference coefficient
Zhang et al. (2020a)	*			*	FA	Fuzzy optimization
Guo et al. (2022)	*			*	NSDE	
Gonzalez et al. (2023)	*		*	*	Borg MOEA	
This Paper	*	*	*	*	NNC	CW-TOPSIS

To resolve the conflicts and formulate a refined short-term operation scheme for CHR that coordinates multiple interests, a complete framework for modeling, solution, and decision-making is urgently needed. However, the following difficulties remain.

### 1. Modeling of short-term multi-objective optimal scheduling (STMOOS)

Due to geographical limitations or the failure to build navigable structures synchronously, not all reservoirs have navigable tasks. How to

precisely satisfy the navigation demands of each HRND while avoiding further expansion of the model scale requires further research. For navigation needs, the literature is either for a single reservoir (Jia et al., 2019), or for the long-term (Zhang et al., 2020b), or as constraints (Diniz and Souza, 2014; Wang and Zhang, 2012), lacking an objective function suitable for STMOOS of CHR.

### 2. Lacking an accurate, stable, and direct solution method for the STMOOS model

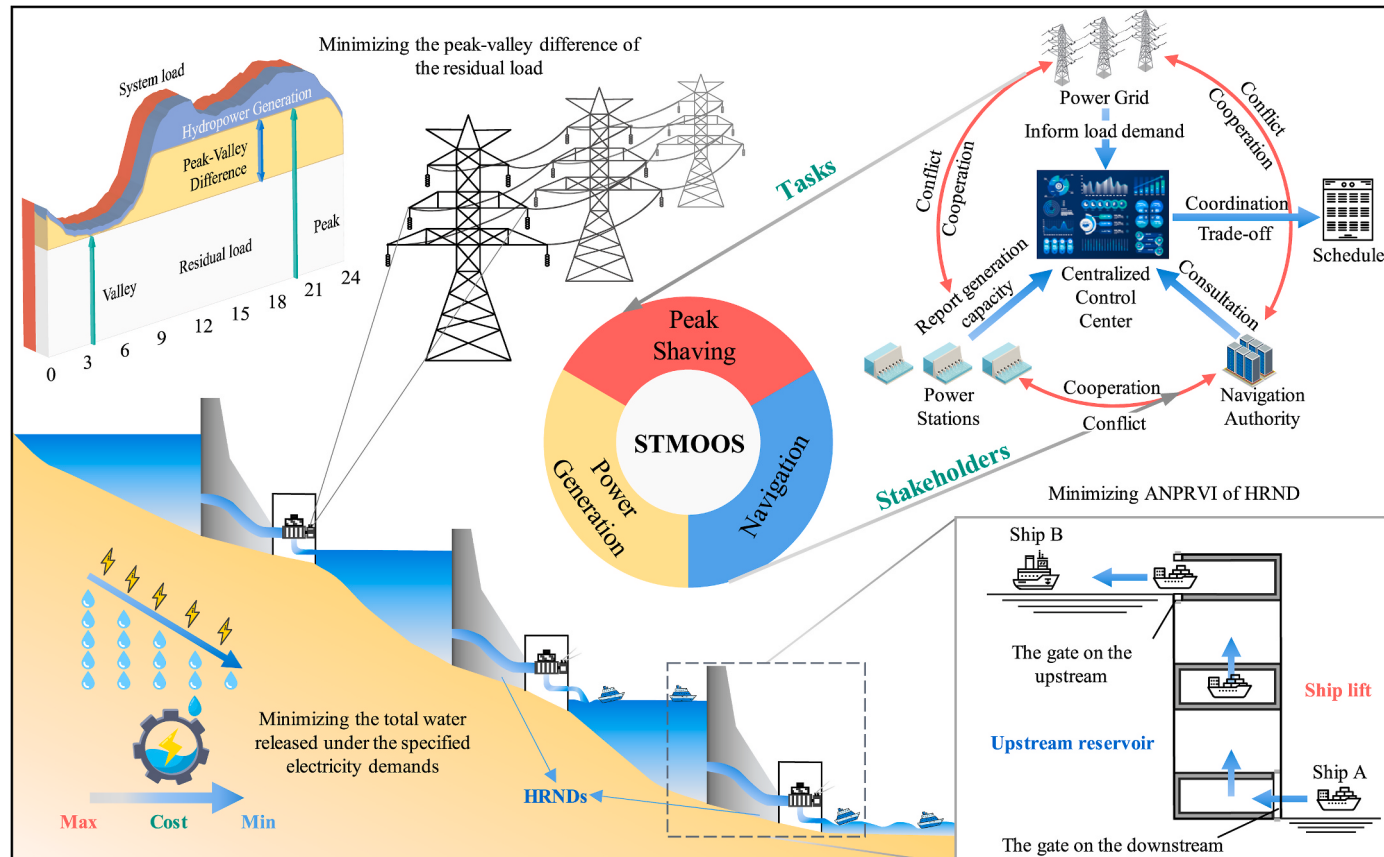


Fig. 1. Schematic diagram of correspondence between stakeholders, operational tasks, and objective functions (Zhao et al., 2020).

The short-term scheduling of CHR is characterized by high dimension, complex constraints, and stricter requirements on the precision and stability of the results (Feng et al., 2019). Compared with unstable and strong random intelligent algorithms, MILP, with its mature theory, stable results, high solution accuracy and user-friendly software is a commonly used method in research and engineering in recent years (Su et al., 2019). However, MILP cannot directly solve MOOPs and needs to handle complex constraints, which requires some improved strategies.

### 3. Selection of decision-making methods

Existing research either stops at obtaining Pareto solutions or uses problem-specific decision-making methods, needing a general approach that considers both subjective and objective preferences.

To address the above challenges, this paper proposes a modeling, solution, and decision-making framework for STMOOS of CHR, with the following main contributions.

1. Propose a navigation objective for HRNDs and combine it with the peak shaving and power generation objectives to build a STMOOS model.
2. Introduce NNC and MILP methods to solve the multi-objective model and obtain Pareto solutions.
3. Utilize the CW-TOPSIS method, which is based on both subjective preference and objective entropy weight, to evaluate the Pareto solutions and determine the final scheduling scheme.

The framework aims to support the Centralized Control Center (CCC) (where information exchange and dispatch coordination occurs) in formulating refined scheduling schemes that coordinate various stakeholders and guide each hydropower reservoir's operation.

The remainder of this paper is organized as follows. Section 2 presents a detailed description of the mathematical formulation of the problem. In Section 3, constraint aggregation and rectangular meshing methods, NNC, and CW-TOPSIS are introduced. The results of the solution and decision-making of the STMOOS are then provided and discussed in Section 4. Finally, Section 5 summarizes the findings and provides the conclusions.

## 2. Problem formulation

**Fig. 1** depicts the correspondence between stakeholders, operational tasks, and objective functions. The modeling in this section is also based on the idea shown in the diagram.

To fully utilize hydropower resources, water spillage is usually avoided in operation, especially in day-ahead scheduling. Without specification, the water spillage will be regarded as zero below, that is, the water discharge is equal to the power release. Additionally, unless otherwise stated,  $n \in N$ ,  $t \in T$  in the following.

### 2.1. Objective functions

This section presents the conceptual and mathematical expressions for the navigation, peak shaving, and power generation objectives.

#### 2.1.1. Navigation objective

Accurate control of tailwater level and water discharge is essential for all HRNDs to improve downstream navigation conditions and meet operational needs of navigable buildings. Since tailwater level is directly affected by water discharge (refer to Eq. (20) and Appendix A for further information) and water discharge is equivalent to power release in the absence of water spillage, limiting power release variations of each HRND can effectively mitigate the negative impact of HPSO. This study proposes the normalized power release variation index (NPRVI) of HRNDs, denoted as  $\psi_t$ , to comprehensively measure the power release fluctuation of all HRNDs, which can be expressed as:

$$\psi_t = \frac{1}{N^D} \sum_{n \in SN^D} |Q_{n,t}^{nor} - \bar{Q}_n^{nor}| \quad (1)$$

$$\bar{Q}_n^{nor} = \frac{1}{T} \sum_{t=1}^T Q_{n,t}^{nor}, \forall n \in SN^D \quad (2)$$

$$Q_{n,t}^{nor} = \frac{Q_{n,t}^{power} - \underline{Q}_{n,t}^{power}}{\bar{Q}_{n,t}^{power} - \underline{Q}_{n,t}^{power}}, \forall n \in SN^D \quad (3)$$

As shown in Eq. (3), the power release of each HRND is normalized first due to their different power release ranges. A smaller NPRVI indicates that the overall power release processes of HRNDs are smoother, and the navigation conditions are better at period  $t$ . Then, by minimizing the average value of NPRVI (ANPRVI,  $\bar{\psi}$  in Eq. (4)) of HRNDs over the scheduling periods, precise control of the variation amplitude and rate of tailwater level can be realized.

$$\min f_1 = \bar{\psi} = \frac{1}{T} \sum_{t=1}^T \psi_t \quad (4)$$

It is worth mentioning that the linearization method adopted in Section 3.1 below aggregates all nonlinear constraints into a power release-related function. Taking the minimization of ANPRVI as the navigation objective function avoids reintroducing the nonlinear constraints of tailwater level-water discharge and reducing computational efficiency.

#### 2.1.2. Peak shaving objective

To regulate the peak loads and smooth the residual load curve, the minimization of the peak-valley difference of the residual load curve is employed as the peak shaving objective function (Wang et al., 2022b), which is described as follows:

$$\min f_2 = \max_{1 \leq t \leq T} (D_t^{res}) - \min_{1 \leq t \leq T} (D_t^{res}) \quad (5)$$

$$D_t^{res} = D_t - \sum_{n=1}^N P_{n,t} \quad (6)$$

#### 2.1.3. Power generation objective

On the premise of satisfying the electricity demand of the power grid and giving full play to the hydropower regulation capacity, minimizing the total operational cost, which is related to the volume of water released from storage, is what power generation enterprises expect. A common operation principle is minimizing the total amount of water released under the specified power demands over the operation periods (Li et al., 2014). The objective function is represented as:

$$\min f_3 = \sum_{n=1}^N \sum_{t=1}^T 3600 \times Q_{n,t}^{out} \times \Delta t \quad (7)$$

## 2.2. Constraints

This section mainly introduces four types of constraints, including reservoir operational constraints, linear and nonlinear constraints on hydropower plant, as well as navigation constraints (Yeh, 1985).

#### 2.2.1. Reservoir operational constraints

##### (1) Continuity balance equation

$$V_{n,t+1} = \begin{cases} V_{n,t} + 3600 \times (Q_{n,t}^{in} - Q_{n,t}^{out}) \Delta t & n = 1 \\ V_{n,t} + 3600 \times (Q_{n,t}^{in} + Q_{n-1,t}^{out} - Q_{n,t}^{out}) \Delta t & n \geq 2 \end{cases} \quad (8)$$

## (2) Storage bounds

$$\underline{V}_n \leq V_{n,t} \leq \bar{V}_n$$

## (3) Initial storage limits

$$V_{n,0} = V_n^{init}$$

## (4) Water discharge limits

$$Q_{n,t}^{out} = Q_{n,t}^{power} + Q_{n,t}^{spill}$$

$$\underline{Q}_n^{out} \leq Q_{n,t}^{out} \leq \bar{Q}_n^{out}$$

$$\underline{Q}_n^{out} = \max(Q_n^{eco}, Q_n^{navi})$$

## 2.2.2. Linear constraints on hydropower plant operation

## (1) Power release bounds

$$\underline{Q}_n^{power} \leq Q_{n,t}^{power} \leq \bar{Q}_n^{power}$$

## (2) Power output bounds

$$\underline{P}_n \leq P_{n,t} \leq \bar{P}_n$$

## (3) Power ramping limits

$$|P_{n,t+1} - P_{n,t}| \leq \Delta P_n$$

## (4) Total electricity demand constraints

$$E = \sum_{n=1}^N \sum_{t=1}^T P_{n,t} \Delta t$$

## (5) Net head constraints

$$H_{n,t} = Z_{n,t} - Z_{n,t}^{tail} - H_{n,t}^{loss}$$

## 2.2.3. Nonlinear constraints on hydropower plant operation

## (1) Water level - storage function

$$Z_{n,t} = f_n^{cv}(V_{n,t})$$

## (2) Tailwater level - water discharge function

$$Z_{n,t}^{tail} = f_n^{tail}(Q_{n,t}^{out})$$

## (3) Head loss - power release function

$$H_{n,t}^{loss} = f_n^{loss}(Q_{n,t}^{power})$$

## (4) Hydropower production function

$$P_{n,t} = f_n^{nhq}(Q_{n,t}^{power}, H_{n,t})$$

## 2.2.4. Navigation constraints

## (1) Hourly variation constraints of the tailwater level

(9)

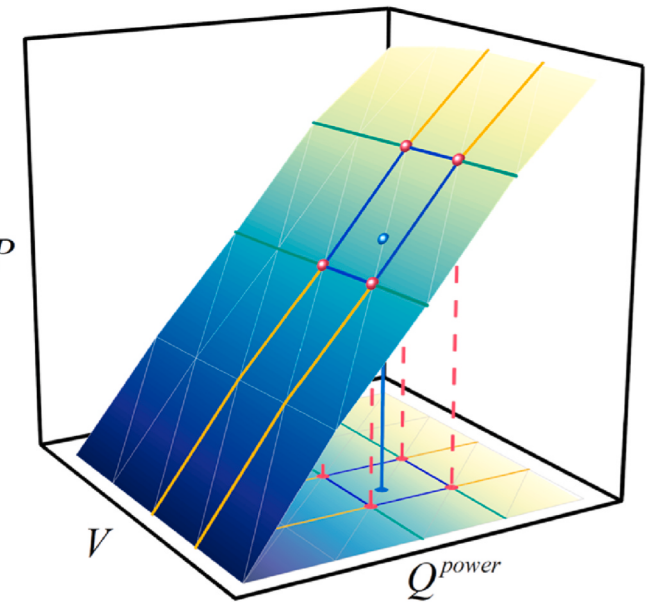


Fig. 2. Equivalent hydropower production function.

(10)

(11)

(12)

(13)

(14)

(15)

(16)

(17)

(18)

(20)

(21)

(22)

$$\Delta Z_{n,t}^h = \left| \frac{Z_{n,t}^{tail} - Z_{n,t-1}^{tail}}{\Delta t} \right|, n \in SN^D, t \in [1, T] \quad (23)$$

## (2) Daily variation constraints of the tailwater level

$$\Delta Z_n^d = \left| \max_{1 \leq t \leq T} (Z_{n,t}^{tail}) - \min_{1 \leq t \leq T} (Z_{n,t}^{tail}) \right|, n \in SN^D \quad (24)$$

Generally, it should restrict the maximum hourly and daily variations of the tailwater level to meet the downstream navigation demands (Diniz and Souza, 2014). Since the navigation objective function has been adopted to satisfy the variation limitations of water discharge and tailwater level, these constraints will be used below as indicators to evaluate the scheme.

## 3. Methodology

This section introduces the linearization, multi-objective optimization, and decision-making methods and finally summarize the overall solution framework.

## 3.1. Nonlinear constraint aggregation and linearization methods

The model's nonlinear constraints Eqs. (19)–(22) remain the primary challenges in STMOOS problem (Zhang et al., 2022). Traditional linearization methods usually perform piecewise linearization for each nonlinear constraint separately, introducing many integer variables. Since the hydropower production function Eq. (22), the main concern in STMOOS problem, is a nonlinear relationship that interconnects the net head, power release, water storage, and power output, the above nonlinear constraints can be aggregated into one function as Eq. (25) shows (Diniz and Maceira, 2008). (Note that  $Q_{n,t}^{out} = Q_{n,t}^{power}$  as described in Section 2.)

$$P_{n,t} = f_n^{nhq}(Q_{n,t}^{power}, f_n^{cv}(V_{n,t}) - f_n^{tail}(Q_{n,t}^{out}) - f_n^{loss}(Q_{n,t}^{power})) = \Gamma_n(Q_{n,t}^{power}, V_{n,t}) \quad (25)$$

Then, the production function of hydropower plant  $n$  is converted into  $\Gamma_n(\cdot)$ , a function of storage, power release, and power output called the equivalent hydropower production function (EHPF) in this paper. The constraint aggregation method can effectively alleviate the conflict

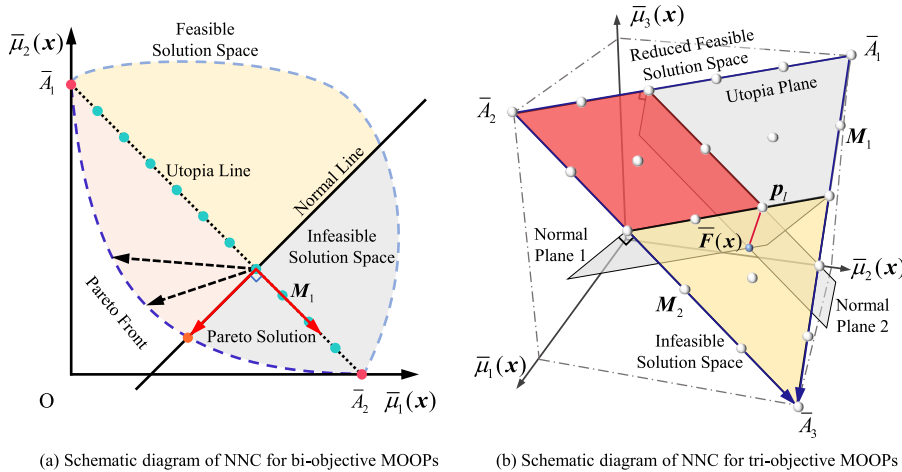


**Fig. 3.** Illustration of NNC for bi-objective and tri-objective MOOPs.

between solution efficiency and precision and guarantees high-precision optimal or nearly-optimal solutions within a reasonable time frame.

As shown in Fig. 2, EHPF is a typical nonlinear three-dimensional surface with independent variables of water storage and power release. To achieve accurate linearization of EHPF, methods such as rectangle and triangle meshing techniques are often adopted, where the surface is divided into several rectangular or triangular grids, and the linear interpolation of any point in space is realized by using the convex combination of grid vertex values. This paper adopts the rectangle meshing method to interpolate the power output of any hydropower plant at any period and the detailed process can be referred to Appendix B.

### 3.2. Normalized normal constraint

After linearizing the nonlinear constraints, a multi-objective MILP model is constructed. The NNC method for solving the MOOP is specified below. Its basic idea is to use the equidistant points on the Utopia hyperplane in the normalized solution space to yield the corresponding uniformly distributed Pareto solutions along the Pareto front. Fig. 3 is an illustration of NNC, and specific procedure can be described as follows:

A common MOOP can be represented as:

$$\min_{x \in \Omega} \{ \mu_1(x), \mu_2(x), \dots, \mu_k(x), \dots, \mu_K(x) \} \quad (26)$$

where  $x$  is the vector of decision variables;  $\Omega$  is the feasible solution space of the MOOP;  $k$  is the index of objectives (unless otherwise specified,  $k = 1, 2, \dots, K$ ); and  $\mu_k(\cdot)$  represents the  $k^{\text{th}}$  objective function.

#### Step 1: Determine the anchor points

The anchor points  $A_k = [\mu_1(x^{k*}), \mu_2(x^{k*}), \dots, \mu_k(x^{k*}), \dots, \mu_K(x^{k*})]$  are generated by individually optimizing each objective function  $\mu_k(x)$ . Here,  $\mu_k(x^{k*})$  denotes the optimum value considering only  $\mu_k(x)$  and  $x^{k*}$  is the corresponding decision variable. The hyperplane, which comprises all the anchor points, is defined as the Utopia hyperplane (or Utopia plane/line).

#### Step 2: Normalize the objective functions

Since the objective functions may have different ranges or physical meanings, it is necessary to map each objective into the normalized space to avoid scaling deficiencies. Therefore, NNC defines the Utopia Point  $F^U$  and Nadir Point  $F^N$  as the mapping parameters to realize the normalized transformation, which are evaluated as follows:

$$F^U = [\mu_1^U \ \mu_2^U \ \dots \ \mu_K^U]^T \quad (27)$$

$$F^N = [\mu_1^N \ \mu_2^N \ \dots \ \mu_K^N]^T \quad (28)$$

where  $\mu_k^U$  and  $\mu_k^N$  are the optimal and worst values of the  $k^{\text{th}}$  objective, called Utopia Value and Nadir Value:

$$\mu_k^U = \mu_k(x^{k*}) \quad (29)$$

$$\mu_k^N = \max [\mu_k(x^{1*}), \mu_k(x^{2*}), \dots, \mu_k(x^{K*})] \quad (30)$$

That is, the Utopia Point can reach the optimum in each objective function, which is practically impossible. Conversely, each objective of the Nadir point is the worst.

Then,  $\bar{\mu}_k(x)$  can be calculated:

$$\bar{\mu}_k(x) = \frac{\mu_k(x) - \mu_k^U}{\mu_k^N - \mu_k^U} \quad (31)$$

#### Step 3: Calculate Utopia Hyperplane Vectors

In the  $K$ -dimensional utopia hyperplane, the vector from point  $\bar{A}_k$  ( $k = 1, 2, \dots, K-1$ ) to point  $\bar{A}_K$ , denoted by  $M_k$ , is defined as follows:

$$M_k = \bar{A}_K - \bar{A}_k \quad (32)$$

where  $\bar{A}_k$  is the normalized anchor points, expressed as:

$$\bar{A}_k = [\bar{\mu}_1(x^{k*}), \bar{\mu}_2(x^{k*}), \dots, \bar{\mu}_k(x^{k*}), \dots, \bar{\mu}_K(x^{k*})] \quad (33)$$

#### Step 4: Decide Normalized Increment

Divide the vector  $M_k$  into  $\delta_k$  segments; correspondingly, the unit length of each segment, i.e., the normalized increment is  $\pi_k = 1/\delta_k$ . To yield an even distribution of points on the  $K$ -dimensional Utopia hyperplane, when given a specified number of points,  $\delta_1$ , along the vector  $M_1$ ,  $\pi_k$  must satisfy:

$$\pi_k = \frac{\pi_1 \|M_k\|}{\|M_1\|} = \pi_1 \quad (34)$$

where  $\|M_k\|$  represents the Euclidean norm of its vector argument  $M_k$ .

#### Step 5: Generate Utopia Hyperplane Points

Additionally, the  $l^{\text{th}}$  point  $p_l$  on the Utopia hyperplane can be

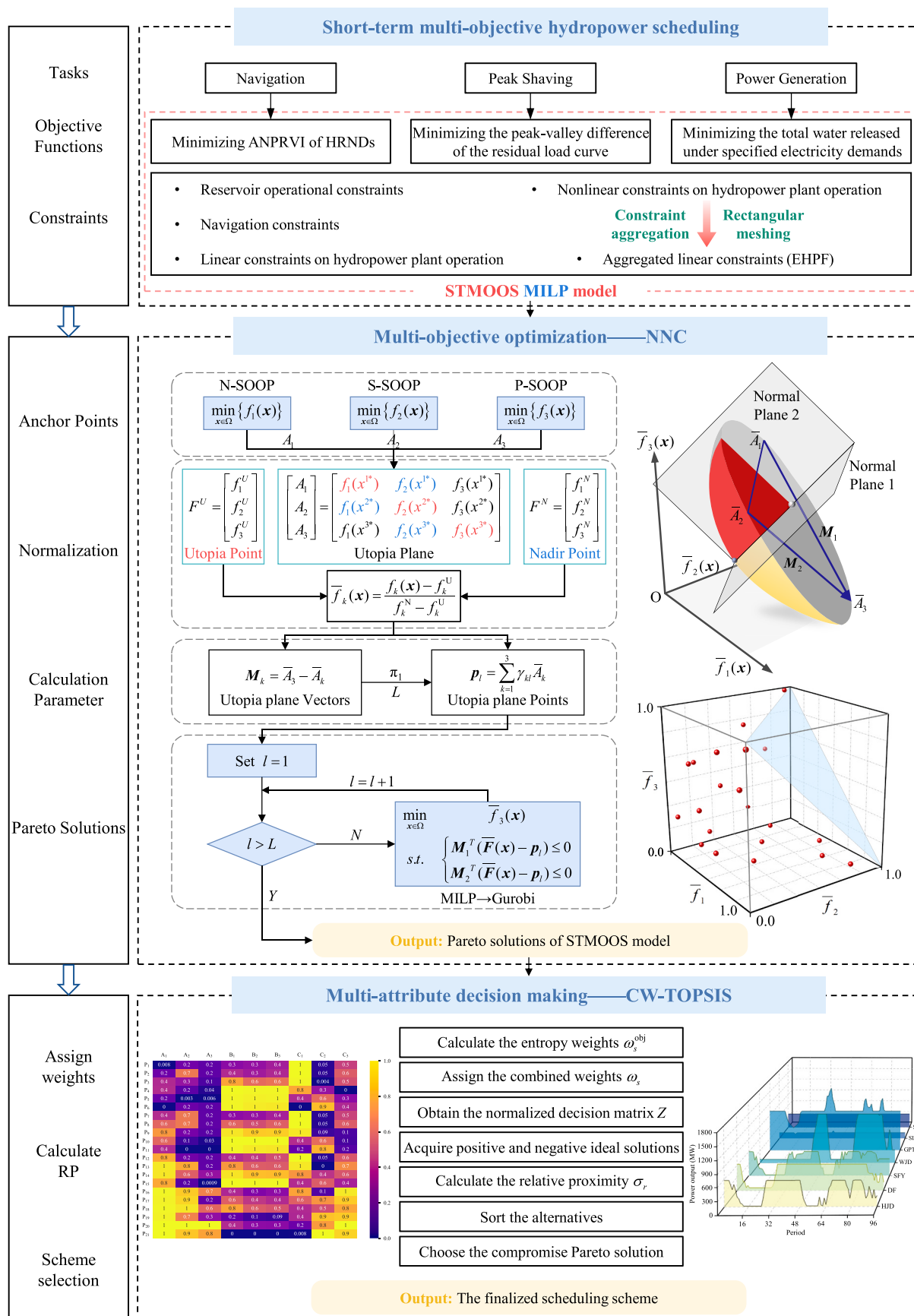


Fig. 4. The solution procedures of modeling, solution and decision-making for STMOOS.

expressed as a convex combination of the normalized anchor points  $\bar{A}_k$ :

$$\mathbf{p}_l = \sum_{k=1}^K \gamma_{kl} \bar{A}_k \quad (35)$$

where  $\gamma_{kl}$  is the combination coefficient,  $0 \leq \gamma_{kl} \leq 1$ ,  $\sum_{k=1}^K \gamma_{kl} = 1$ ;  $l = 1, 2, \dots, L$ .

#### Step 6: Obtain the Pareto Solutions

For each point generated in Step 5, the corresponding Pareto solution can be obtained by solving the following problem Eqs. (36) and (37), and then a set of well-distributed Pareto solutions are yielded in the normalized objective space.

$$\min_{x \in \Omega} \bar{\mu}_K(\mathbf{x}) \quad (36)$$

subject to:

$$\mathbf{M}_k^T (\bar{\mathbf{F}}(\mathbf{x}) - \mathbf{p}_l) \leq 0 \quad (1 \leq k \leq K - 1) \quad (37)$$

where:

$$\bar{\mathbf{F}}(\mathbf{x}) = [\bar{\mu}_1(\mathbf{x}), \bar{\mu}_2(\mathbf{x}), \dots, \bar{\mu}_K(\mathbf{x})]^T \quad (38)$$

#### Step 7: Restore Pareto solutions' actual metric values

The actual metric values of the Pareto solutions obtained in Step 6 can be restored by the following equation:

$$\mu_k = \bar{\mu}_k \cdot (\mu_k^N - \mu_k^U) + \mu_k^U \quad (39)$$

To facilitate understanding, an explanation of NNC for bi-objective problems is provided. In Fig. 3(a),  $\bar{A}_1, \bar{A}_2$  are anchor points in the normalized space, and  $M_1$  is the Utopia Line Vector. Along  $M_1$ , equidistant points  $\mathbf{p}_l$  ( $l = 1, 2, \dots, L$ ) are taken, and normals to  $M_1$  are drawn through each  $\mathbf{p}_l$ . A normal constraint (Eq. (37)) corresponding to each  $\mathbf{p}_l$  is added to the original problem, which makes the gray area below the normal infeasible (gray area has been explored by previous points). Under this constraint, the Pareto solution that corresponds to  $\mathbf{p}_l$  is determined, characterized as making  $\bar{\mu}_2$  minimal and being as close to Utopia Point  $O$  as possible.  $L$  Pareto solutions can be obtained by iteratively solving Eq. (36) with updated normal constraint Eq. (37). The finer the Utopia Line is divided, the closer the resulting Pareto solutions set is to the true Pareto front. The tri-objective problem shown in Fig. 3 (b) and the  $k$ -objective problem shown in Eq. (26) are similar and not discussed further.

#### 3.3. CW-TOPSIS decision-maker

The Pareto solutions of the problem can be obtained through the above method, i.e., a series of scheduling schemes. To evaluate each scheme and make a trade-off between different objectives, CW-TOPSIS is introduced for decision-making.

As a classical multi-attribute decision-making method, TOPSIS ranks alternatives by calculating their relative distance from positive and negative ideal solutions. When applying TOPSIS, the determination of attribute weights is essential. An approach that can balance objective information and subjective intentions is expected (Chen, 2021). Therefore, a combined weighting method is adopted, using the entropy method integrated subjective preference to assign objective and subjective weights to attributes, which avoids excessive reliance on data diversity in objective weighting and the arbitrariness of subjective weighting. Specific steps for TOPSIS can be referred to in previous reports (Hwang and Yoon, 1981) and Appendix C.

In this study, each scheme can be regarded as an alternative, and the value of each objective function corresponding to the solution can be

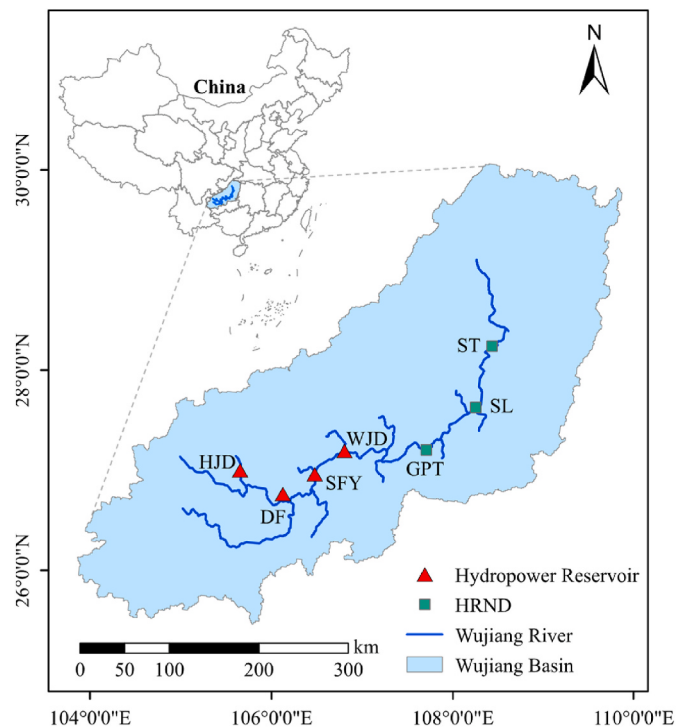


Fig. 5. The geographic distribution of the Wujiang CHR.

considered an indicator. Additionally, since the normalized Pareto front is obtained in Step 6 of NNC, Step 7 of NNC and Step 1 of CW-TOPSIS can be omitted here. The actual value of the compromise solution can be restored through Eq. (39) after making the final decision.

#### 3.4. Solution procedure

The overall procedure of modeling, solution, and decision-making for STMOOS is given in Fig. 4. Please note that when determining the anchor point in the first step of NNC, it should conduct single-objective optimization with each sub-objective serving as the objective function. For simplicity, N-SOOP, S-SOOP, and P-SOOP will be referred to as the SOOP of navigation, peak shaving, and power generation. Additionally, it is worth noting that the advanced Gurobi optimizer (Gurobi Optimization, LLC, 2022) is used to solve the transformed MILP model, primarily employing inner point and branch and bound methods.

#### 4. Case study

The proposed framework is applied to the STMOOS of CHR in Wujiang River, Southwest China. After presenting the fundamental data of CHR related to the model, three case studies are conducted to verify the framework's effectiveness and obtain a quarter-hourly operation schedule balancing the benefits of peak shaving, power generation, and navigation. The simulation experiments are conducted using Python 3.8.1 and Gurobi 9.5.1, running on an Intel(R) Core(TM) i5-8250U CPU @ 1.60 GHz.

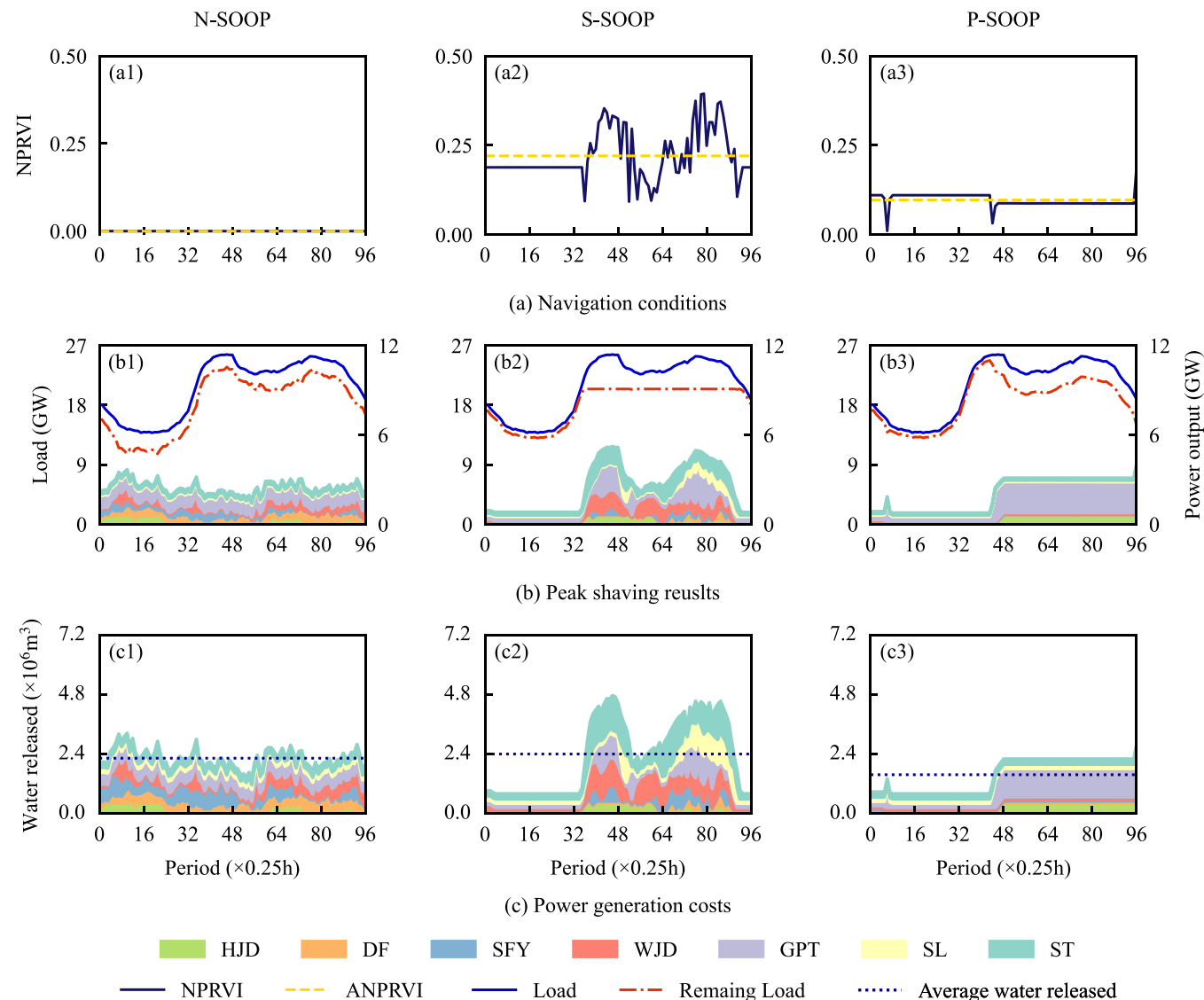
##### 4.1. Cascade hydropower reservoirs in Wujiang River

The Wujiang River, abundant in hydropower and water resources, is a crucial hydropower base and an inland waterway. With a total installed capacity of 8315 MW, the seven hydropower plants built on the trunk stream of the Wujiang River are important peak-shaving power sources for the Guizhou Power Grid. GPT to ST is the navigable river section with a total mileage of 410.8 km. The geographic distribution of the CHR in Wujiang River is shown in Fig. 5 and Table 2 lists the basic

**Table 2**

Basic data of CHR in Wujiang River.

Hydropower reservoir	Regulating ability	Installed capacity (MW)	Ramping capacity (MW)	Forebay level bounds (m)	Water release bounds ( $m^3/s$ )	Power release bounds ( $m^3/s$ )	EHPF interval number
HJD	Carryover	600	200	[1076,1140]	[14.4,3866]	[0,490]	$4 \times 4$
DF	Seasonal	695	232	[936,970]	[77,11142]	[0,632]	$4 \times 4$
SFY	Daily	600	200	[822,835]	[77,15956]	[0,990]	$4 \times 4$
WJD	Seasonal	1250	417	[720,760]	[112,18360]	[0,1200]	$4 \times 4$
GPT	Annual	3000	1000	[590,630]	[190,23560]	[0,1909]	$4 \times 4$
SL	Daily	1050	350	[431,440]	[193,25737]	[0,1772]	$4 \times 4$
ST	Daily	1120	373	[353,5360]	[228,27500]	[0,1969]	$4 \times 4$

**Fig. 6.** Comparison of SOOP results for different objectives in dry season scenario.

parameters of the hydropower reservoirs (Yeh, 1985).

#### 4.2. Case 1: comparison of the results of SOOPs and MOOPs under different scenarios

In this case, the NNC-MILP method is utilized to solve the aforementioned multi-objective model for dry and flood season scenarios to validate the proposed model and methods. As previously stated, the calculation parameters (including anchor points, Utopia Value, Nadir

Value, etc.) of NNC will be first obtained by optimizing N-SOOP, S-SOOP, and P-SOOP separately. The results will also verify the conflicts between navigation, peak shaving, and power generation.

Figs. 6–7 below are the results in the dry and flood season scenarios. Fig. 6(a)–(c) show the results of navigation, peak-shaving, and power generation under each SOOP in turn; the subplots from left to right in Fig. 6(a)–(c) are the results of the N-SOOP, S-SOOP, and P-SOOP separately. For example, Fig. 6(b3) shows the peak shaving results of the P-SOOP. Fig. 7 is arranged analogously while detailed data is provided

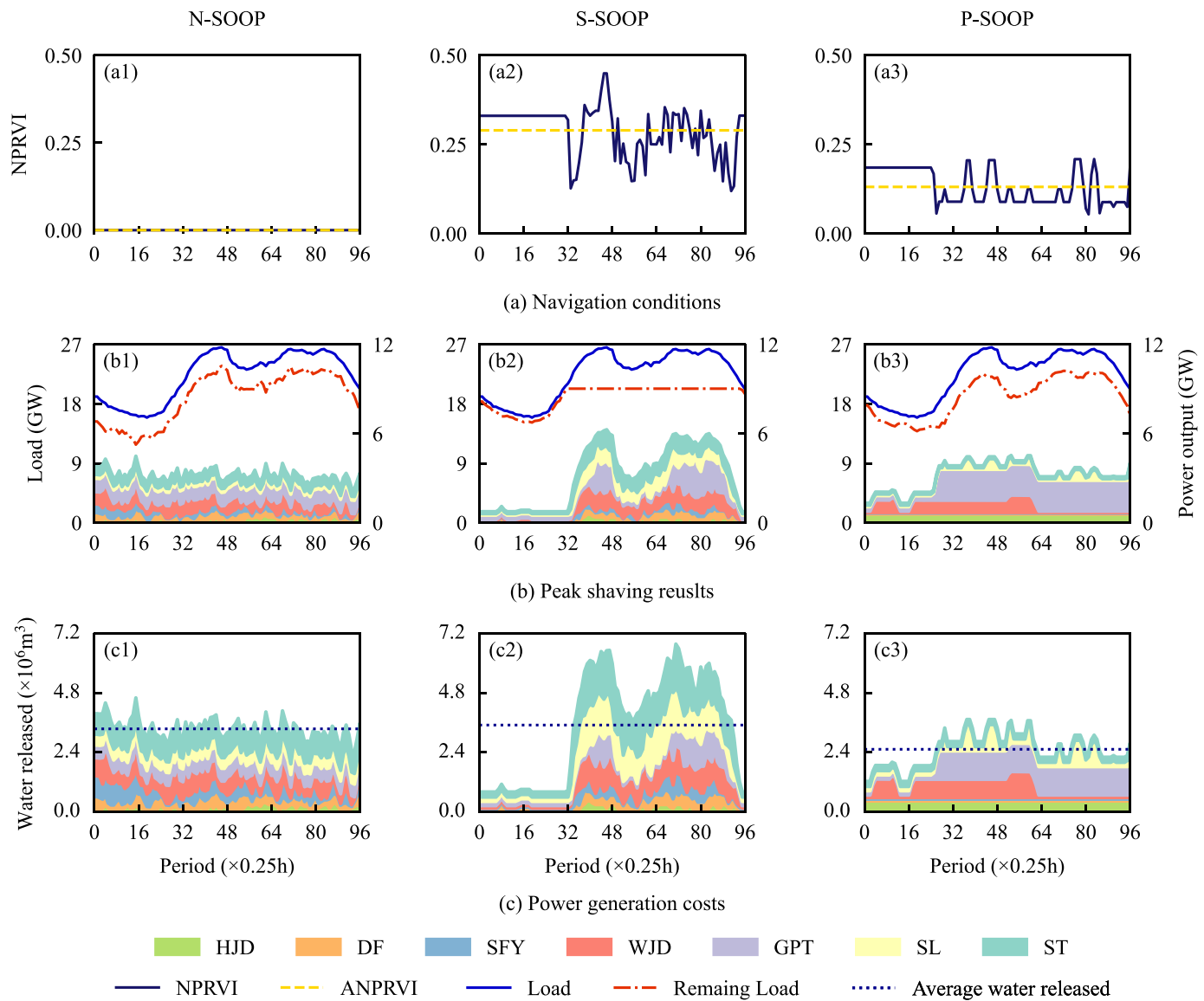


Fig. 7. Comparison of SOOP results for different objectives in flood season scenario.

**Table 3**  
SOOP results for different objectives in dry and flood season scenarios.

Scenarios	Objective Value	N-SOOP	S-SOOP	P-SOOP	Utopia Value	Nadir Value
Dry season	$f_1$	0.000	0.220	0.097	0.000	0.220
	$f_2$ (GW)	13.123	7.426	11.401	7.426	13.123
	$f_3$ ( $10^8 \text{ m}^3$ )	2.149	2.310	1.794	1.794	2.310
Flood season	$f_1$	0.000	0.290	0.131	0.000	0.290
	$f_2$ (GW)	11.912	5.124	9.136	5.124	11.912
	$f_3$ ( $10^8 \text{ m}^3$ )	3.217	3.363	2.424	2.424	3.363

in Table 3. Additionally, Figs. 6-7(a) only represents the overall navigation conditions of HRNDs ( $n \in SN^D$ ); detailed water discharge processes in N-SOOP are provided in Appendix D to validate the navigation objective.

The results shown in the chart are analyzed as follows.

#### 1. HPSO will destroy the navigation conditions.

Fig. 6(a) presents that ANPRVI is minimum in N-SOOP and

maximum in S-SOOP, while NPRVI has a large variation amplitude and rate in S-SOOP, reaching values up to 0.30 and 0.88/h. Additionally, as shown in Fig. 6(b) and Table 3, S-SOOP has the peak-valley difference of residual load at 7425.59 MW, whereas N-SOOP has the maximum at 13123.22 MW, indicating a 76.73% increase. These results demonstrate a significant contradiction between peak shaving and navigation.

#### 2. HPSO will increase the total water released for power generation.

Fig. 6(c) and Table 3 show that P-SOOP has the lowest total water released at  $2.424 \times 10^8 \text{ m}^3$ , while S-SOOP has the highest at  $3.363 \times 10^8 \text{ m}^3$ , indicating a 38.74% increase, which reveals that HPSO will increase total water released for power generation. The reason can be inferred from Fig. 6(b). To minimize the peak-valley difference of residual load, all hydropower plants lower output during valley load period ( $t = 16$ ) and increase it during peak load periods ( $t = 48, t = 80$ ) in S-SOOP. However, to minimize total water released in P-SOOP, GPT, HJD, and ST are prioritized for power generation due to their higher efficiency and lower water consumption, while other plants operate close to or at zero. These results confirm that CHR faces conflicting operational requirements between peak shaving and power generation tasks.

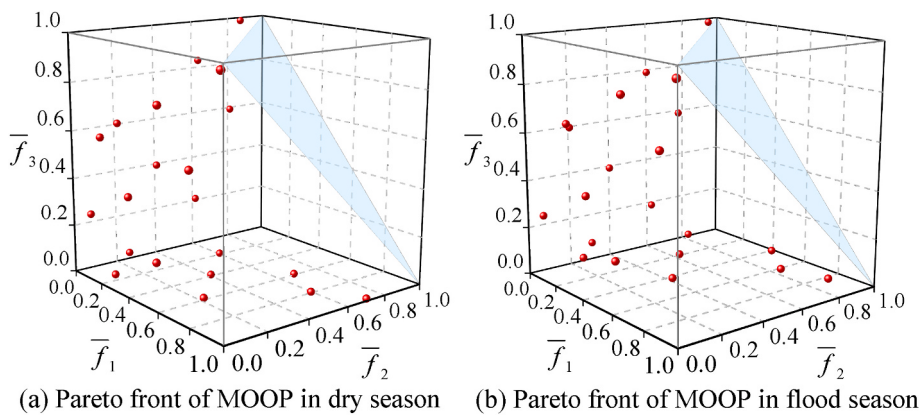
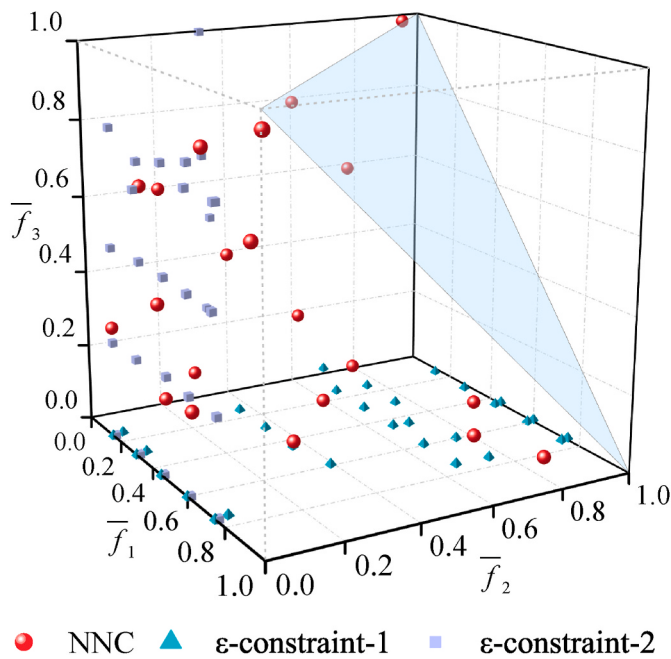


Fig. 8. The Pareto fronts of MOOPs in the normalized space.



**Fig. 9.** Pareto fronts obtained through NNC and  $\epsilon$ -constraint methods. (Note:  $\epsilon$ -constraint-1,  $\epsilon$ -constraint-2 denote  $\epsilon$ -constraint methods taking power generation and peak shaving as main objective function.)

3. Navigation and power generation targets are also in conflict.

**Fig. 6(a1), (a3), (c1), and (c3)** demonstrate the presence of a conflict between navigation and power generation, although this conflict is relatively less pronounced than the contradictions with HPSO.

These observations underline the need to develop a model and framework that can effectively coordinate the conflicts among navigation, peak shaving, and power generation. The results obtained for flood scenario, as depicted in **Fig. 7**, validate similar contradictions.

**Fig. 8(a) and (b)** present the Pareto fronts obtained using NNC-MILP method. The blue planes in these figures represent the Utopia plane, while each point corresponds to a scheme. The results demonstrate that ideal solutions for dry and flood seasons can be obtained. Additionally, the solutions are distributed evenly and widely, which effectively captures the restrictive relationship between different objectives. It is worth mentioning that the solution density and computational burden need to be balanced according to actual needs. Overall, the Pareto front obtained through NNC-MILP provides a useful tool for decision-makers to balance conflicting objectives and make informed decisions regarding

**Table 4**  
Weights of each objective.

	Objective 1	Objective 2	Objective 3
Subjective weight	0.5000	0.2500	0.2500
Entropy weight	0.3548	0.2740	0.3712
Combined weight	0.5238	0.2022	0.2740

Note: Objective 1, 2, and 3 represent navigation, peak shaving, and power generation.

CHR operation.

#### 4.3. Case 2: comparison of different multi-objective solution methods

To assess the effectiveness of the NNC method in solving STMOOS problem, taking dry season scenario as an example, the WS,  $\epsilon$ -constraint, and NNC methods are compared. The results reveal that the WS cannot obtain an optimal solution in a reasonable time for the problem, and the final gap (see **Appendix D**) is far beyond the tolerance. **Fig. 9** highlights a significant difference between the Pareto fronts obtained using NNC and  $\epsilon$ -constraint methods, with the latter displaying an uneven distribution and mainly concentrated in a single dimension. Additionally, the results of choosing different objective functions as the main objective function are quite disparate, which cannot describe the trade-off between the objectives accurately. In contrast, the Pareto front obtained by the NNC has an extensive and uniform distribution, which is superior to that of the  $\epsilon$ -constraint method. These findings confirm the effectiveness of the NNC in solving STMOOS problem and its ability to handle complex, conflicting objectives in a comprehensive and efficient manner.

#### 4.4. Case 3: decision-making on pareto solutions

The CW-TOPSIS method is further applied for decision-making on the Pareto solutions of the flood season scenario in Case 1. Here, a situation that navigation is more demanding is assumed. **Table 4** shows the weights assigned to each objective. Considering the significance of subjective weights, brief sensitivity analysis results are provided in **Appendix D**.

**Fig. 10** illustrates the normalized decision matrix of the Pareto solutions and each scheme's relative proximity calculated using three methods: traditional subjective weighting TOPSIS (SW-TOPSIS), entropy weighting TOPSIS (EW-TOPSIS), and CW-TOPSIS. Detailed results are tabulated in **Table 5**.

It can be observed that schemes 13, 14, and 13 has the highest relative proximity in SW-TOPSIS, EW-TOPSIS, and CW-TOPSIS, with corresponding values of 0.8482, 0.8299, and 0.8446. Although SW-TOPSIS and CW-TOPSIS finalized the same scheme, the latter considered the diversity of objective data, avoiding arbitrary decision-making.

	$f_1$	$f_2$	$f_3$	SW	EW	CW
1	0.5617	0.1823	0.9974	0.5580	0.5497	0.5542
2	0.5679	0.3125	1.0000	0.5832	0.5909	0.5817
3	0.5636	0.7582	0.9897	0.6498	0.7409	0.6584
4	0.3295	1.0000	0.8024	0.5154	0.6714	0.5324
5	0.1173	0.9974	0.4029	0.3714	0.5213	0.3908
6	0.1003	0.9998	0.0077	0.3317	0.4429	0.3491
7	0.5631	0.2184	0.9969	0.5645	0.5602	0.5613
8	0.5654	0.5363	0.9957	0.6188	0.6670	0.6225
9	0.4609	0.9507	0.9582	0.6021	0.7388	0.6159
10	0.1862	0.9879	0.5933	0.4193	0.5800	0.4384
11	0.0000	0.9925	0.2001	0.3197	0.4585	0.3389
12	0.5892	0.3089	0.9969	0.5945	0.5939	0.5921
13	0.8720	0.7235	0.9596	0.8482	0.8245	0.8446
14	0.8382	0.9403	0.7506	0.8332	0.8299	0.8336
15	0.3159	0.9852	0.3923	0.4519	0.5610	0.4666
16	0.9657	0.2990	0.7896	0.7414	0.6219	0.7253
17	1.0000	0.5398	0.6015	0.7799	0.6673	0.7671
18	0.9675	0.7571	0.3929	0.7629	0.6565	0.7526
19	0.9999	0.0823	0.4029	0.6509	0.4772	0.6311
20	0.8810	0.2692	0.1679	0.6125	0.4395	0.5945
21	0.9815	0.0000	0.0000	0.5812	0.3897	0.5607

**Fig. 10.** CW-TOPSIS results. (Note: 1–21 are the number of the schemes; SW, EW, and CW denote the relative proximity calculated through TOPSIS, EW-TOPSIS, and CW-TOPSIS.)

**Table 5**  
Comparison of the results obtained through different methods.

	S-SOOP	SW-TOPSIS	EW-TOPSIS	CW-TOPSIS	Improvement
Scheme	—	13	14	13	—
$f_1$	0.290	0.010	0.048	0.010	96.54%
$f_2$ (GW)	5.124	6.550	5.184	6.550	-27.82%
$f_3$ ( $10^8 \text{m}^3$ )	3.363	2.997	3.172	2.997	10.88%

Note: Improvement item denote the improvement between CW-TOPSIS results and original S-SOOP results.

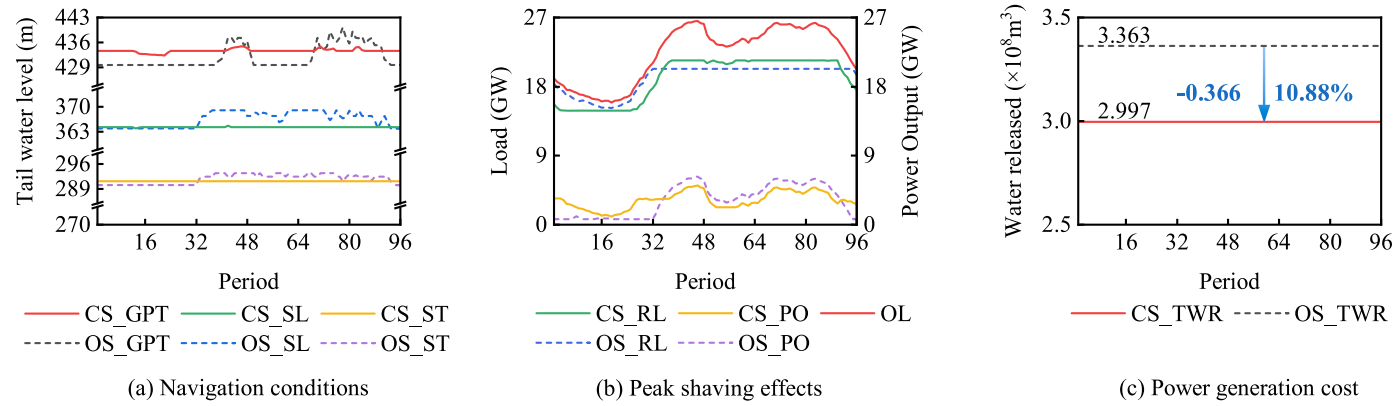


**Fig. 11.** Comparison of the results of CS and OS. (Note: RL: Residual load; PO: Power output; OL: Original load; TWR: Total water released.)

Additionally, if no subjective preference were introduced, EW-TOPSIS would tend to choose the scheme with better peak-shaving benefits, contrary to the decision-makers' expectations.

Therefore, the compromise scheme (CS) extracted by CW-TOPSIS

can be determined as Scheme 13. Fig. 11 compares the results of the CS with the S-SOOP (abbreviated as the original scheme, OS).

Fig. 11(a) displays the navigable conditions of the HRNDs, demonstrating that the tailwater level variation of each HRND is effectively

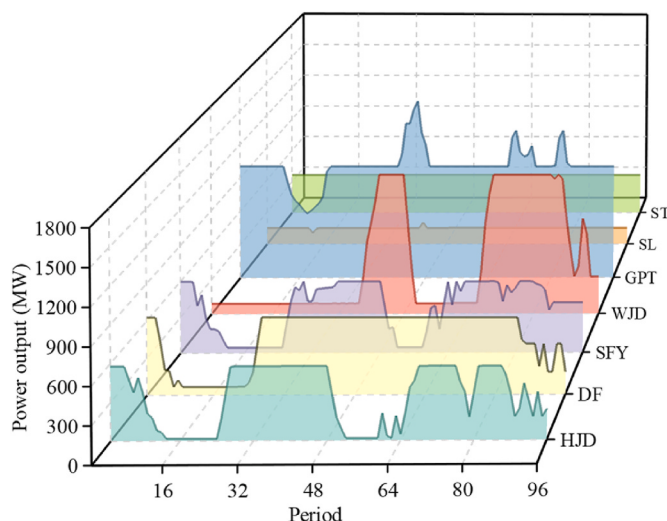


**Fig. 12.** Quarter-hourly power output processes of CS.

controlled. The maximum hourly tailwater level variations of GPT, SL, and ST are 3.81 m/h, 1.66 m/h, and 0.004 m/h, which mark reductions of 75.46%, 84.53%, 98.82%, while the maximum daily tailwater level variations are 2.58 m/d, 0.78 m/d, and 0.04 m/d, decreased by 76.13%, 81.88%, 99.93%, both meeting the requirements better. Fig. 11(b) illustrates that the CS loses part of the peak shaving benefits, with an increase of 27.82% in the peak-valley difference of the remaining load, which is unavoidable but still responds to the overall load demand and maintains the peak shaving effect. Additionally, Fig. 11(c) indicates a 10.88% decrease in total water released, suggesting an improvement in power generation efficiency.

Fig. 12 presents the power output process of each hydropower plant in the CS, i.e., the final quarter-hourly operation schedule acquired through the study's framework.

## 5. Conclusion

This paper proposes a multi-objective optimization model for resolving the apparent contradictions among peak shaving, navigation, and power generation in the short-term scheduling of CHR. To accurately characterize the navigation demand of HRNDs, a novel navigation objective function that minimizes the ANPRVI of HRNDs is proposed. The Pareto solutions of the model are obtained by NNC-MILP method, and the final scheduling scheme is determined using CW-TOPSIS. Application to the day-ahead scheduling of the Wujiang CHR validates several conclusions.

1. The case study's results of NNC-MILP solving STMOOS in flood and dry seasons in Section 4.2 indicate that there are significant conflicts among peak shaving, power generation, and navigation in both dry

and flood seasons, which must be considered, and the negative impact of peak shaving on power generation and navigation is particularly pronounced.

2. The comparison of different multi-objective solution methods in Section 4.3 shows that the results obtained using NNC are distributed more widely and evenly than those obtained by commonly used scalarization MOOP methods, demonstrating its effectiveness.
3. The comparison between the results of CS and OS in Section 4.4 suggests that the proposed framework based on NNC-MILP and CW-TOPSIS methods can resolve hydropeaking-navigation-production conflicts of CHR efficiently.

The above explanation shows that the presented model can accurately describe the interests of various stakeholders, and the proposed framework can effectively obtain Pareto solutions and make reasonable decisions. The accurate quarter-hourly generation schedules of CHR formulated using the framework provide a valuable reference for the operation of CCC and CHR, and have crucial practical significance. However, this paper still has deficiencies. It fails to resolve the conflict between density of Pareto solutions and computational efficiency in NNC, and does not consider the impact of renewables integration (such as wind and solar) on CHR operation. Future research could focus on these issues, such as introducing parallel technology or analyzing uncertain factors originating from wind and solar.

## CRediT authorship contribution statement

**Xiangyu Ma:** Methodology, Software, Writing – original draft. **Shengli Liao:** Conceptualization, Writing – review & editing, Funding acquisition. **Benxi Liu:** Data curation, Formal analysis. **Hongye Zhao:** Validation, Visualization. **Chuntian Cheng:** Supervision, Resources. **Huaying Su:** Investigation, Resources.

## Declaration of competing interest

The authors declare that they have no known competing financial interests or personal relationships that could have appeared to influence the work reported in this paper.

## Data availability

Data will be made available on request.

## Acknowledgements

The work was supported by the National Natural Science Foundation of China (No. 51979023, No. U1765103) and the Open Research Fund of Hubei Key Laboratory of Intelligent Yangtze and Hydroelectric Science (No. ZZH2302017). We would like to thank the editors and anonymous reviewers for their constructive comments and suggestions.

## Appendix A

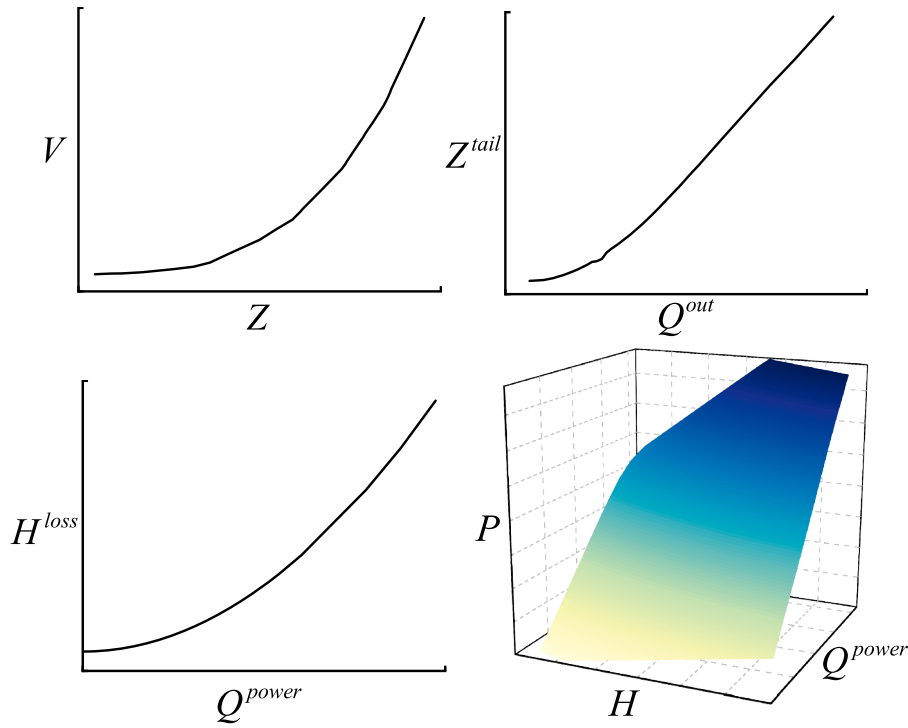


Fig. A1. Nonlinear relationship functions.

## Appendix B

For clarity, the subscripts  $n$  and  $t$  will be omitted below in this subsection, and  $V$ ,  $Q$ , and  $P$  represent  $V_{n,t}$ ,  $Q_{n,t}^{power}$ , and  $P_{n,t}$ . Similarly,  $\bar{V}$ ,  $\underline{V}$ ,  $\bar{Q}$ , and  $\underline{Q}$  represent  $\bar{V}_n$ ,  $\underline{V}_n$ ,  $\bar{Q}_n^{power}$ , and  $\underline{Q}_n^{power}$ .

Fig. B1 is a diagram of the projection of the EHPF surface shown in Fig. 2 on the storage – power release plane. A discrete  $(I+1) \times (J+1)$  grid related to the power output is obtained by discretizing the storage  $V$  and power release  $Q$  into  $I$  and  $J$  segments within their respective ranges.

$$\underline{V} = \hat{V}_0 < \hat{V}_1 < \dots < \hat{V}_I = \bar{V} \quad (\text{B.1})$$

$$\underline{Q} = \hat{Q}_0 < \hat{Q}_1 < \dots < \hat{Q}_J = \bar{Q} \quad (\text{B.2})$$

Each grid vertex corresponds to the power output  $\hat{P}_{i,j}$ , and the weight of each vertex  $\lambda_{i,j}$  is assigned.  $\alpha_i$  and  $\beta_j$  are the sums of the weights of a discrete vertex in the vertical and horizontal directions.

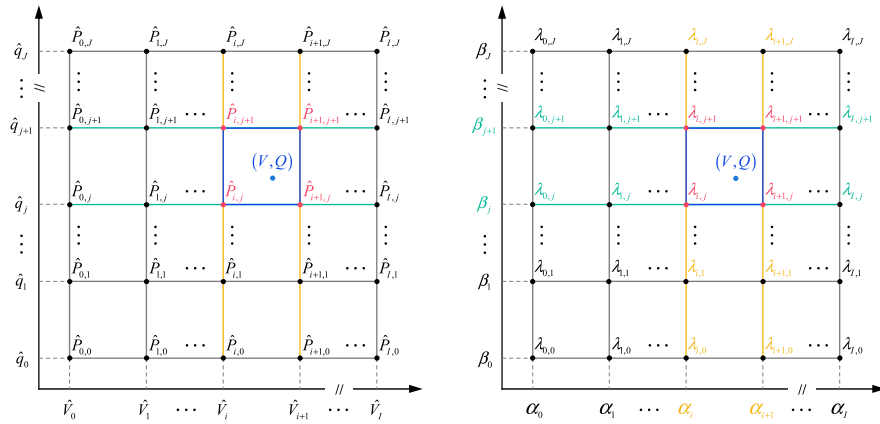


Fig. B1. Projection of EHPF on the storage-power release plane.

$$\sum_{i=0}^I \sum_{j=0}^J \lambda_{i,j} = 1, \lambda_{i,j} \geq 0 \quad (\text{B.3})$$

$$\alpha_i = \sum_{j=0}^J \lambda_{ij}, \forall i \in [0, I] \quad (\text{B.4})$$

$$\beta_j = \sum_{i=0}^I \lambda_{ij}, \forall j \in [0, J] \quad (\text{B.5})$$

To avoid introducing a large number of integer variables, Eq. (B.6) introduces the SOS2 constraint, which allows up to two consecutive variables to take nonnegative values while all other variables must be zero. The power output of hydropower plants can then be calculated using Eqs. (B.7)-(B.9), where  $\widehat{P}_{ij}$  is a constant,  $\widehat{P}_{ij} = \Gamma(\widehat{q}_j, \widehat{V}_i)$ .

$$\text{SOS2}\left(\{\alpha_i\}_{i \in [0, I]}\right), \text{SOS2}\left(\{\beta_j\}_{j \in [0, J]}\right) \quad (\text{B.6})$$

$$\sum_{i=0}^I \alpha_i \widehat{V}_i = V \quad (\text{B.7})$$

$$\sum_{j=0}^J \beta_j \widehat{Q}_j = Q \quad (\text{B.8})$$

$$\sum_{i=0}^I \sum_{j=0}^J \lambda_{ij} \widehat{P}_{ij} = P \quad (\text{B.9})$$

## Appendix C

The CW-TOPSIS decision-making method consists following steps:

First, the initial data matrix with  $R$  evaluation alternatives and  $S$  evaluation indicators is set as follows:

$$Y = \begin{bmatrix} o_{1,1} & o_{1,2} & \cdots & o_{1,S} \\ o_{2,1} & o_{2,2} & \cdots & o_{2,S} \\ \vdots & \vdots & \ddots & \vdots \\ o_{R,1} & o_{R,2} & \cdots & o_{R,S} \end{bmatrix} \quad (\text{C.1})$$

where  $o_{r,s}$  denotes the value of the  $r^{th}$  alternative in the  $s^{th}$  indicator,  $r = 1, 2, \dots, R$ ,  $s = 1, 2, \dots, S$ .

### Step 1: Data Normalization

Since there are two types of indicators, cost-based (the smaller the better) and benefit-based (the larger the better), and the indicators may have different ranges and units, all indicators need to be normalized to benefit-based indicators within the  $[0, 1]$  interval first.

$$y_{r,s} = \begin{cases} \frac{o_{r,s} - \min(o_{r,s})}{\max(o_{r,s}) - \min(o_{r,s})}, o_{r,s} \text{ is } \text{ind}^+ \\ \frac{\max(o_{r,s}) - o_{r,s}}{\max(o_{r,s}) - \min(o_{r,s})}, o_{r,s} \text{ is } \text{ind}^- \end{cases} \quad (\text{C.2})$$

where  $\text{ind}^+$  and  $\text{ind}^-$  represent benefit-based and cost-based indicators.

### Step 2: Calculate the entropy weights

Due to the advantages of enhancing the distinction of indicators, fully reflecting data information and not relying on subjective preferences, the entropy weighing method is frequently used for objective weight determination for TOPSIS. The calculation steps are as follows:

$$\tau_{r,s} = \frac{y_{r,s}}{\sum_{r=1}^R y_{r,s}} \quad (\text{C.3})$$

$$e_s = -\frac{1}{\ln R} \sum_{r=1}^R \tau_{r,s} \ln \tau_{r,s}, (s = 1, 2, \dots, S) \quad (\text{C.4})$$

$$\omega_s^{\text{obj}} = \frac{1 - e_s}{S - \sum_{s=1}^S e_s} \quad (\text{C.5})$$

where  $y_{r,s}$  is the normalized value of  $o_{r,s}$ ;  $\tau_{r,s}$  is the proportion of the  $s^{th}$  index of  $y_{r,s}$ , a nonnegative constant;  $e_s$  is the information entropy value of the  $s^{th}$

indicator,  $0 \leq e_s \leq 1$ ; when  $\tau_{r,s} = 0$ , set  $\tau_{r,s} \ln \tau_{r,s} = 0$ ; and  $\omega_s^{\text{obj}}$  is the entropy weight of the  $s^{\text{th}}$  indicator.

### Step 3: Assign the combined weights

When faced with different scheduling situations, there is indeed a priority among the indicators. To avoid overreliance on objective information leading to deviation from decision-makers' needs, subjective preferences should be considered. The subjective weights are introduced here, and the combined weighting method is used to assign the weights.

$$\omega_s = \frac{\omega_s^{\text{subj}} \cdot \omega_s^{\text{obj}}}{\sum_{s=1}^S \omega_s^{\text{subj}} \cdot \omega_s^{\text{obj}}} \quad (\text{C.6})$$

where  $\omega_s^{\text{subj}}$  is the subjective weight of the  $s^{\text{th}}$  indicator,  $\omega_s$  is the combined weight of the  $s^{\text{th}}$  indicator,  $0 \leq \omega_s \leq 1$ , and  $\sum_{s=1}^S \omega_s = 1$ .

### Step 4: Calculate the relative proximity (RP) by TOPSIS

Through Eq. (C.7), the combined weighted normalized decision matrix  $Z$  is obtained.

$$Z = \begin{bmatrix} G_1 & \left[ z_{1,1} & z_{1,2} & \cdots & z_{1,S} \right] \\ G_2 & \left[ z_{2,1} & z_{2,2} & \cdots & z_{2,S} \right] \\ \vdots & \vdots & \ddots & \vdots \\ G_R & \left[ z_{R,1} & z_{R,2} & \cdots & z_{R,S} \right] \end{bmatrix} \quad (\text{C.7})$$

where:

$$z_{r,s} = \omega_s y_{r,s} \quad (\text{C.8})$$

Additionally, the positive and negative ideal solutions can be acquired as:

$$G^+ = [z_1^+, z_2^+, \dots, z_S^+] \quad (\text{C.9})$$

$$G^- = [z_1^-, z_2^-, \dots, z_S^-] \quad (\text{C.10})$$

where  $z_s^+ = \max(z_{1,s}, z_{2,s}, \dots, z_{R,s})$ ,  $z_s^- = \min(z_{1,s}, z_{2,s}, \dots, z_{R,s})$ .

Then the distance from the positive ideal solution  $d_r^+$  or negative ideal solution  $d_r^-$  to each alternative  $G_r$  and the relative proximity  $\sigma_r$  can be calculated:

$$d_r^+ = \sqrt{\sum_{s=1}^S (z_{r,s} - z_s^+)^2}, d_r^- = \sqrt{\sum_{s=1}^S (z_{r,s} - z_s^-)^2} \quad (\text{C.11})$$

$$\sigma_r = \frac{d_r^-}{d_r^+ + d_r^-} \quad (\text{C.12})$$

where  $0 \leq \sigma_r \leq 1$ .

### Step 5: Sorting the alternatives

Now, alternatives can be ranked in descending order of the value of relative proximity  $\sigma_r$ . The one with the highest proximity value will be the most appropriate choice, i.e., the best compromise solution in the Pareto front.

## Appendix D

The Gurobi's MILP solver will terminate when the gap between the lower and upper objective bound is less than the Gap times the absolute value of the incumbent objective value, which can be expressed as:

$$\text{gap} = \frac{\text{objective solution} - \text{lower objective bound}}{\text{lower objective bound}} \times 100\% \quad (\text{D.1})$$

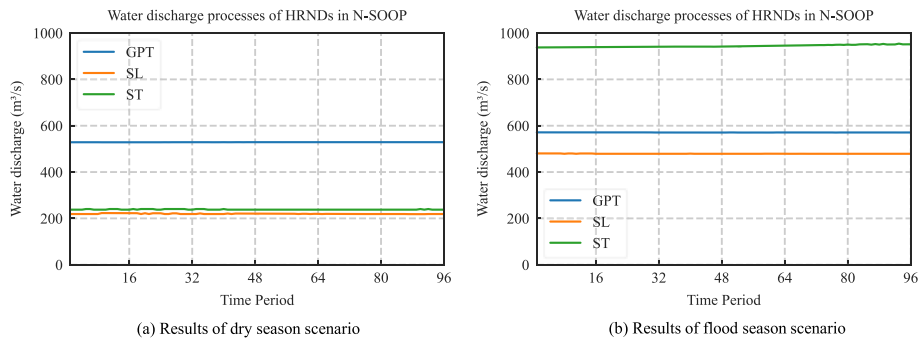


**Fig. D1.** Water discharge processes of HRNDs.

In Fig. D2, Rows 1–21 illustrate scheduling schemes, and the columns denote various subjective weight (SW) combinations for each objective. Each cell presents the relative proximity of a given scheme under the corresponding weight combination, which was calculated using CW-TOPSIS. The improvement rate of objectives 1–3 between CS and OS is shown in Rows 23–25.

**Fig. D2.** Sensitivity analysis results of subjective weights.

## References

- Alkan, O., Albayrak, O.K., 2020. Ranking of renewable energy sources for regions in Turkey by fuzzy entropy based fuzzy COPRAS and fuzzy MULTIMOORA. Renew. Energy 162, 712–726. <https://doi.org/10.1016/j.renene.2020.08.062>.

Anindito, Y., Haas, J., Olivares, M., Nowak, W., Kern, J., 2019. A new solution to mitigate hydropeaking? Batteries versus re-regulation reservoirs. J. Clean. Prod. 210, 477–489. <https://doi.org/10.1016/j.jclepro.2018.11.040>

- Branche, E., 2017. The multipurpose water uses of hydropower reservoir: the SHARE concept. *C. R. Phys.* 18, 469–478. <https://doi.org/10.1016/j.crhy.2017.06.001>.

Bruder, A., Tonolla, D., Schweizer, S.P., Vollenweider, S., Langhans, S.D., Wüest, A., 2016. A conceptual framework for hydropeaking mitigation. *Sci. Total Environ.* 568, 1204–1212. <https://doi.org/10.1016/j.scitotenv.2016.05.032>.

Chen, P., 2021. Effects of the entropy weight on TOPSIS. *Expert Syst. Appl.* 168, 114186 <https://doi.org/10.1016/j.eswa.2020.114186>.

- Ding, N., Duan, J., Xue, S., Zeng, M., Shen, J., 2015. Overall review of peaking power in China: status quo, barriers and solutions. *Renew. Sustain. Energy Rev.* 42, 503–516. <https://doi.org/10.1016/j.rser.2014.10.041>.
- Diniz, A.L., Macceira, M.E.P., 2008. A four-dimensional model of hydro generation for the short-term hydrothermal dispatch problem considering head and spillage effects. *IEEE Trans. Power Syst.* 23, 12981308 <https://doi.org/10.1109/TPWRS.2008.922253>.
- Diniz, A.L., Souza, T.M., 2014. Short-term hydrothermal dispatch with river-level and routing constraints. *IEEE Trans. Power Syst.* 29, 2427–2435. <https://doi.org/10.1109/TPWRS.2014.2300755>.
- Feng, Z., Niu, W., Cheng, C., 2017. Multi-objective quantum-behaved particle swarm optimization for economic environmental hydrothermal energy system scheduling. *Energy* 131, 165–178. <https://doi.org/10.1016/j.energy.2017.05.013>.
- Feng, Z., Niu, W., Cheng, C., 2019. China's large-scale hydropower system: operation characteristics, modeling challenge and dimensionality reduction possibilities. *Renew. Energy* 136, 805–818. <https://doi.org/10.1016/j.renene.2019.01.059>.
- Ghiasi, H., Pasini, D., Lessard, L., 2010. Pareto frontier for simultaneous structural and manufacturing optimization of a composite part. *Struct. Multidiscip. Optim.* 40, 497–511. <https://doi.org/10.1007/s00158-009-0366-4>.
- Gonzalez, J.M., Tomlinson, J.E., Martínez Cesena, E.A., Basheer, M., Obuobie, E., Padi, P.T., Addo, S., Baisie, R., Etchia, M., Hurford, A., Bottacin-Busolin, A., Matthews, J., Dalton, J., Smith, D.M., Sheffield, J., Panteli, M., Harou, J.J., 2023. Designing diversified renewable energy systems to balance multisector performance. *Nat. Sustain.* <https://doi.org/10.1038/s41893-022-01033-0>.
- Guo, Y., Ming, B., Huang, Q., Wang, Y., Zheng, X., Zhang, W., 2022. Risk-averse day-ahead generation scheduling of hydro-wind-photovoltaic complementary systems considering the steady requirement of power delivery. *Appl. Energy* 309, 118467. <https://doi.org/10.1016/j.apenergy.2021.118467>.
- Gurobi Optimization, L.L.C., 2022. Gurobi Optimizer Reference Manual. <https://www.gurobi.com>. (Accessed 1 March 2023).
- Hwang, C.L., Yoon, K.P., 1981. Multiple Attribute Decision Making. Methods and Applications. A State-Of-The-Art Survey. Springer. <https://doi.org/10.1007/978-3-642-48318-9>.
- IHA, 2022. Hydropower status report. <https://www.hydopower.org/status-report>. (Accessed 28 February 2023).
- Jia, T., Qin, H., Yan, D., Zhang, Z., Liu, B., Li, C., Wang, J., Zhou, J., 2019. Short-term multi-objective optimal operation of reservoirs to maximize the benefits of hydropower and navigation. *Water* 11, 1272. <https://doi.org/10.3390/w11061272>.
- Kling, H., 2017. Climate variability risks for electricity supply. *Nat. Energy* 2, 916–917. <https://doi.org/10.1038/s41560-017-0059-y>.
- Li, X., Li, T., Wei, J., Wang, G., Yeh, W.W.G., 2014. Hydro unit commitment via mixed integer linear programming: a case study of the three gorges project, China. *IEEE Trans. Power Syst.* 29, 1232–1241. <https://doi.org/10.1109/TPWRS.2013.2288933>.
- Li, Y., Fu, X., Chu, X., Liu, S., 2022. A conflict resolution model for reservoir operation in dry seasons under channel alteration. *J. Hydrol.* 610, 127899 <https://doi.org/10.1016/j.jhydrol.2022.127899>.
- Liao, S., Liu, H., Liu, B., Zhao, H., Wang, M., 2022. An information gap decision theory-based decision-making model for complementary operation of hydro-wind-solar system considering wind and solar output uncertainties. *J. Clean. Prod.* 348, 131382. <https://doi.org/10.1016/j.jclepro.2022.131382>.
- Liao, S., Liu, Z., Liu, B., Cheng, C., Wu, X., Zhao, Z., 2021. Daily peak shaving operation of cascade hydropower stations with sensitive hydraulic connections considering water delay time. *Renew. Energy* 169, 970–981. <https://doi.org/10.1016/j.renene.2021.01.072>.
- Moreira, M., Hayes, D.S., Boavida, I., Schletterer, M., Schmutz, S., Pinheiro, A., 2019. Ecologically-based criteria for hydropeaking mitigation: a review. *Sci. Total Environ.* 657, 1508–1522. <https://doi.org/10.1016/j.scitotenv.2018.12.107>.
- Moura De Figueiredo, N., Cavalcante Blanco, C.J., Pinheiro Campos Filho, L.C., Amarante Mesquita, A.L., 2023. Muwos - multiple use water optimization system for the power generation and navigation trade-offs analysis. *Renew. Energy* 203, 205–218. <https://doi.org/10.1016/j.renene.2022.12.004>.
- Pereira, R.B.D., Leite, R.R., Alvim, A.C., Paiva, A.P.D., Ferreira, J.R., Davim, J.P., 2017. Multi-objective robust optimization of the sustainable helical milling process of the aluminum alloy al 7075 using the augmented-enhanced normalized normal constraint method. *J. Clean. Prod.* 152, 474–496. <https://doi.org/10.1016/j.jclepro.2017.03.121>.
- Poff, N.L., Schmidt, J.C., 2016. How dams can go with the flow. *Science* 353, 1099–1100. <https://doi.org/10.1126/science.aaa4926>.
- Sahin, O., Stewart, R.A., Giurco, D., Porter, M.G., 2017. Renewable hydropower generation as a co-benefit of balanced urban water portfolio management and flood risk mitigation. *Renew. Sustain. Energy Rev.* 68, 1076–1087. <https://doi.org/10.1016/j.rser.2016.01.126>.
- Shang, Y., Li, X., Gao, X., Guo, Y., Ye, Y., Shang, L., 2017. Influence of daily regulation of a reservoir on downstream navigation. *J. Hydrol. Eng.* 22, 05017010 <https://doi.org/10.1016/j.jhydrol.2014-5584.0001522>.
- Shen, J.J., Cheng, C.T., Wang, S., Yuan, X.Y., Sun, L.F., Zhang, J., 2020. Multiobjective optimal operations for an interprovincial hydropower system considering peak-shaving demands. *Renew. Sustain. Energy Rev.* 120, 109617 <https://doi.org/10.1016/j.rser.2019.109617>.
- Simab, M., Javadi, M.S., Nezhad, A.E., 2018. Multi-objective programming of pumped-hydro-thermal scheduling problem using normal boundary intersection and VIKOR. *Energy* 143, 854–866. <https://doi.org/10.1016/j.energy.2017.09.144>.
- Su, C., Cheng, C., Wang, P., Shen, J., Wu, X., 2019. Optimization model for long-distance integrated transmission of wind farms and pumped-storage hydropower plants. *Appl. Energy* 242, 285293. <https://doi.org/10.1016/j.apenergy.2019.03.080>.
- Uddin, M., Romlie, M.F., Abdullah, M.F., Abd Halim, S., Abu Bakar, A.H., Chia Kwang, T., 2018. A review on peak load shaving strategies. *Renew. Sustain. Energy Rev.* 82, 3323–3332. <https://doi.org/10.1016/j.rser.2017.10.056>.
- Wang, H.R., Li, F.F., Wang, G.Q., Qiu, J., 2022a. Shrinking pareto fronts to guide reservoir operations by quantifying competition among multiple objectives. *Water Resour. Res.* 58, e2021WR029702 <https://doi.org/10.1029/2021WR029702>.
- Wang, J., Zhang, Y., 2012. Short-term optimal operation of hydropower reservoirs with unit commitment and navigation. *J. Water Resour. Plan. Manage.-ASCE* 138, 3–12. [https://doi.org/10.1016/\(ASCE\)WR.1943-5452.0000142](https://doi.org/10.1016/(ASCE)WR.1943-5452.0000142).
- Wang, P., Yuan, W., Su, C., Wu, Y., Lu, L., Yan, D., Wu, Z., 2022b. Short-term optimal scheduling of cascade hydropower plants shaving peak load for multiple power grids. *Renew. Energy* 184, 68–79. <https://doi.org/10.1016/j.renene.2021.10.079>.
- Wang, X., Dong, Z., Ai, X., Dong, X., Li, Y., 2020. Multi-objective model and decision-making method for coordinating the ecological benefits of the Three Gorges Reservoir. *J. Clean. Prod.* 270, 122066 <https://doi.org/10.1016/j.jclepro.2020.122066>.
- Yang, Z., Yang, K., Wang, Y., Su, L., Hu, H., 2020. Multi-objective short-term hydropower generation operation for cascade reservoirs and stochastic decision making under multiple uncertainties. *J. Clean. Prod.* 276, 122995 <https://doi.org/10.1016/j.jclepro.2020.122995>.
- Yeh, W.W., 1985. Reservoir management and operations models: a state-of-the-art review. *Water Resour. Res.* 21, 1797–1818. <https://doi.org/10.1029/WR021i012p01797>.
- Yu, L., Wu, X., Wu, S., Jia, B., Han, G., Xu, P., Dai, J., Zhang, Y., Wang, F., Yang, Q., Zhou, Z., 2021. Multi-objective optimal operation of cascade hydropower plants considering ecological flow under different ecological conditions. *J. Hydrol.* 601, 126599 <https://doi.org/10.1016/j.jhydrol.2021.126599>.
- Zhang, H., Chang, J., Gao, C., Wu, H., Wang, Y., Lei, K., Long, R., Zhang, L., 2019. Cascade hydropower plants operation considering comprehensive ecological water demands. *Energy Convers. Manag.* 180, 119133 <https://doi.org/10.1016/j.enconman.2018.10.072>.
- Zhang, X., Huang, W., Chen, S., Xie, D., Liu, D., Ma, G., 2020a. Grid-source coordinated dispatching based on heterogeneous energy hybrid power generation. *Energy* 205, 117908. <https://doi.org/10.1016/j.energy.2020.117908>.
- Zhang, Z., Qin, H., Yao, L., Liu, Y., Jiang, Z., Feng, Z., Ouyang, S., 2020b. Improved multi-objective moth-flame optimization algorithm based on r-domination for cascade reservoirs operation. *J. Hydrol.* 581, 124431 <https://doi.org/10.1016/j.jhydrol.2019.124431>.
- Zhang, Z., Wu, X., Liao, S., Cheng, C., 2022. An ultra-short-term scheduling model for cascade hydropower regulated by multilevel dispatch centers suppressing wind power volatility. *Int. J. Electr. Power Energy Syst.* 134, 107467 <https://doi.org/10.1016/j.ijepes.2021.107467>.
- Zhao, X., Lin, Q., Yu, H., 2020. A co-scheduling problem of ship lift and ship lock at the Three Gorges Dam. *IEEE Access* 8, 132893–132910. <https://doi.org/10.1109/ACCESS.2020.3009775>.
- Zhou, L., Cheng, C., Liao, S., Wang, J., 2020. Multiobjective scheduling method for short-term peak shaving operation of cascade hydro plants. *J. Water Resour. Plan. Manage.-ASCE* 146, 04020073 [https://doi.org/10.1016/\(ASCE\)WR.1943-5452.0001274](https://doi.org/10.1016/(ASCE)WR.1943-5452.0001274).